

This is the pre-published version.

Efficient Visible Light Photocatalytic Oxidation of NO on F, N Codoped Spherical TiO₂ Synthesized via Ultrasonic Spray Pyrolysis

Jianhui Huang,^{a, c} * Wahkit Cheuk,^c Yifan Wu,^b Frank S. C. Lee^b, Wingkei Ho,^{b, c} *

a. Environmental and Life Sciences Department, Putian University, Putian 351100, China;

b. Department of Civil and Structural Engineering, Research Center for Environmental Technology and Management, The Hong Kong Polytechnic University, Hong Kong.

c. Nano and Advanced Materials Institute Limited, The Hong Kong University of Science & Technology, Hong Kong, P. R. China;

* Corresponding authors.

Email: owenhuang95@163.com, howingkei@gmail.com

Abstract

Fluorine and nitrogen codoped TiO₂ was synthesized by ultrasonic spray pyrolysis method using titanium tetrafluoride and urea as F and N precursors, respectively. The codoped TiO₂ was characterized by X-ray diffractometry (XRD), scanning electron microscopy (SEM), transmission electron microscopy (TEM), diffuse reflectance spectroscopy (DRS), and X-ray photoelectron spectroscopy (XPS). Photocatalytic oxidation of nitric oxide (NO) in gas-phase medium was employed as a probe reaction to evaluate the photocatalytic reactivity of the catalysts. The results indicated that spherical codoped TiO₂ photocatalysts with unique puckered surface was obtained by this method. This codoped catalysts have solely anatase crystalline structure. The photocatalytic measurement showed that the codoped catalysts could efficiently oxidize NO under visible light irradiation with wavelength in the range of 400 to 550 nm. The formation mechanism of the codoped TiO₂ is also discussed.

1. Introduction

Growing knowledge on the indoor air quality (IAQ) has validated it as one of the major risks of the human health as people spend more than 80% of their time indoors in most countries [1]. Thus, more and more attentions have been drawn into developing a green process of eliminating pollutants from indoor air. Several physical and chemical methods for treating the indoor air pollutants have been studied extensively, including adsorption [2,3], ozonation [4], plasma [5] and photocatalytic oxidation [6-9]. Among these, semiconductor-mediated photocatalysis is one of the most efficient technologies because of its high redox ability, non-selectivity and flexibility of reaction condition, i.e. at room temperature and atmospheric pressure. For decades, titanium dioxide (TiO_2) has been one of the most promising photocatalysts owing to its intrinsic properties such as low cost, high chemical stability and low toxicity. Unfortunately, a major obstacle in the popularization of TiO_2 is its large band gap (3.2 eV) which work only under specific UV light region ($\lambda < 380$ nm), hence practically ruling out most of the solar energy for the environmental remediation. Thus, considerable efforts have been devoted to the modified TiO_2 in order to broaden the light response range of TiO_2 -base photocatalysts, which is still a significant issue in both academic and practical applications. Doping TiO_2 with various elements has been proved as an effective method to optimize the band structure of TiO_2 , and thereby resulting to be a visible-light sensitive photocatalyst. The cationic doping TiO_2 is often impaired by thermal instability and an increase in the population of recombination centers, thus no significant results were achieved. [10,11] Doping TiO_2 with non-metal such as N, C, S, B, P seems to be more efficient to address this problem. [12-18] Among them, doping with nitrogen atom is considered to be one of the most effective way to obtain visible-light-driven photocatalytic activity. [19,20] However, the reactivity or quantum efficiency of only doping nitrogen is still not high enough. Many researches were designed to codope with other non metal elements such as C, S, B, P [21-24] via the synergistic effects between two dopants in

order to further enhance the photocatalytic efficiency. Among them, intense interest has been shown on the F, N codoped TiO₂. [25-30] The fluorine doping would result in the formation of reduced Ti³⁺ ions and surface oxygen vacancies, which may promote charge separation and improve the efficiency of photoinduced processes. Thus the synergistic effects between the N and F dopants may effectively enhance the photocatalytic efficiency of single N doped TiO₂.

Synthetic methods such as solgel and hydrothermal technique have been widely used to synthesize the codoped TiO₂ photocatalyst, which can precise control of pore structure, dopant concentration, and chemical purity [31-33]. However, they require severe conditions such as long time for reaction or equipment with high pressure resistance, which is not easy in large scale production. Thus, a high-yield synthetic method that is capable of producing nanostructure TiO₂ with controllable dopant concentration and crystallinity will undoubtedly benefit the design of high-performance catalytic materials in the industry. Ultrasonic spray pyrolysis is a convenient method for the facile mass production of nanostructured spherical materials because of its simple, inexpensive apparatus and easy control of product composition. Recently, carbon, SiO₂, Bi₂WO₆, InVO₄, etc. have been synthesized by this method. [34-37] Although ultrasonic spray pyrolysis has been widely used to produce inorganic powders, it is still a challenge to fabricate the material with heteroatom especially the nonmetal atoms.

In this study, we fabricated fluorine and nitrogen codoped TiO₂ using ultrasonic spray pyrolysis method with urea and titanium tetrafluoride as precursors. The as-prepared product had unique spherical structures with puckered surface and exhibited high photocatalytic activity on the oxidation of NO in air under the irradiation of visible light. The preparation method is simple and continuous which is easy for batch production. Moreover, the dopants of such TiO₂ sphere can be easily controlled by regulating the experimental conditions.

2. Experimental section

2.1 Catalysts preparation

All of the chemicals were commercially available analytical grade and used without further purification. Fluorine and nitrogen codoped TiO₂ photocatalysts were prepared by an ultrasonic spray pyrolysis method. In a typical process, TiF₄ (1.5 g) was added to 150 mL HCl solution (0.5 M) under magnetic stirring. After stirring for several minutes, a transparent colorless solution was obtained. Then, different quantity of urea (0, 1, 5 and 10 g) was added to the solution under magnetic stirring. After the urea was dissolved completely, the resulting solution was nebulized at 1.7 MHz \pm 10% (YUYUE402AI, Shanghai). The produced aerosol was carried with pumping air flow (5 L/min) through a quartz tube surrounded by a furnace thermostated. The pyrolysis proceeded quickly as aerosol passed through the high-temperature tube maintained at the temperature of 500 °C. The quartz reaction tube with the diameter of 3.5 cm was 1 m long. The products were collected in a percolator with distilled water, then separated by centrifugation, washed thoroughly with ethanol and distilled water, and finally dried in an oven at 100 °C for 1 h. A vivid yellow product was obtained. The as prepared produced was then further calcinated at 500 °C and held for 1 h (ramp rate of 1 °C/min). The samples prepared by addition of 1 g, 5 g and 10 g urea were designated FNT-1, FNT-5, and FNT-10 respectively. For comparison, the fluorine doped TiO₂ was also prepared without adding urea was designated FT.

2.2 Characterization

The X-ray diffraction (XRD) patterns were recorded on a Bruker D8 Advance X-ray diffractometer with Cu K α radiation ($\lambda = 1.54178 \text{ \AA}$) at a scan rate of 0.05° 2 θ /s. The accelerating voltage and the applied current were 40 kV and 40 mA, respectively. Scanning electron microscopy (SEM, JSM-5600) was used to characterize the morphology of the obtained products. Transmission electron microscopy (TEM) study was carried out on a Philips CM- 120 electron microscopy instrument. The samples for TEM were prepared by dispersing the final powders in methanol; the

dispersion was then dropped on carbon copper grids. A Varian Cary 100 Scan UV – Visible system equipped with a Labsphere diffuse reflectance accessory was used to obtain the reflectance spectra of the catalysts over a range of 200 - 800 nm. Labsphere USRS-99-010 was employed as a reflectance standard. The spectra were converted from reflection to absorbance by Kubelka – Munk method. X-ray photoelectron spectroscopy (XPS) measurements were performed on a PHI Quantum 2000 XPS System with a monochromatic Al K α source and a charge neutralizer. All the binding energies were calibrated to the C 1s peak at 284.8 eV of the surface adventitious carbon.

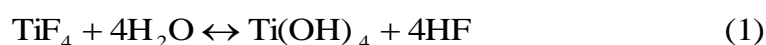
2.3 NO removal test

The nitric oxide (NO) is the common pollutant of indoor air. It was reported by WHO that it could cause respiratory symptoms, bronchoconstriction, increased bronchial reactivity, airway inflammation and decreases in immune defence leading to increased susceptibility to respiratory infection. Thus, we used NO photocatalytic oxidation to evaluate the performance of photocatalysts in this study. The NO removal with the resulting samples was performed at ambient temperature in a continuous flow reactor. The volume of the rectangular reactor which was made of stainless steel and covered with Saint-Glass was 4.5 L (10 cm \times 30 cm \times 15 cm (H \times L \times W)). The sample to be tested was prepared by coating an aqueous suspension of the photocatalyst onto a dish with a diameter of 5.0 cm. The weight of the photocatalysts used for each experiment was kept at 0.3 g. The dishes containing the photocatalyst were pretreated at 70 °C for several hours until a complete removal of water in the suspension and then cooled to room temperature before use. The lamp was vertically placed outside the reactor above the sample dish, and a glass filter was placed to cutoff light below 400 nm. Four mini fans were fixed around the lamp to avoid the temperature rise of the flow system. Furthermore, adequate distance was also kept from the lamp to the reactor for the same purpose to avoid temperature rise. The NO gas was acquired from compressed gas cylinder at a concentration of 48 ppm NO (N₂ balance, BOC gas) with traceable National Institute of Standards and

Technology (NIST) standard. The initial concentration of NO was diluted to about 400 ppb by the air stream supplied by a zero air generator (Thermo Environmental Inc. Model 111). The desired humidity level of the NO flow was controlled at 70% (2100 ppmv) by passing the zero air streams through a humidification chamber. The gas streams were pre-mixed completely by a gas blender and the flow rate was controlled at 4 L min⁻¹ by a mass flow controller. After the adsorption – desorption equilibrium among water vapor, gases and photocatalysts was achieved, the lamp was turned on. The concentration of NO was continuously measured by a chemiluminescence NO analyzer (Thermo Environmental Instruments Inc. Model 42c), which monitors NO, NO₂, and NO_x (NO_x represents NO + NO₂) with a sampling rate of 0.7 L min⁻¹. The reaction of NO with air was ignorable when performing a control experiment with or without light in the absence of photocatalyst.

3 Result and discussion

Fig. 1 shows the XRD patterns of the prepared samples. All the samples exhibit five distinct peaks ($2\theta = 25.4, 38.1, 48.1, 53.9, \text{ and } 55.6^\circ$) which represent the indices of (101), (004), (200), (105) and (211) planes of anatase TiO₂. The crystalline sizes of the samples prepared by adding 0, 1, 5 and 10 g urea estimated by Scherrer formula from the (101) peaks of anatase phase were 14, 13, 10 and 9 nm, respectively. This indicates that TiO₂ particles in the prepared samples are nanocrystalline in nature. The result also evidences the addition of urea could suppress undesirable sintering and agglomeration of TiO₂ particle during the thermal treatment. In this process, TiO₂ nanoparticle possibly formed via the following two consecutive reaction steps.



In the absence of urea, the rate of hydrolysis and condensation reactions (eq. (1) and eq. (2)) are rather slow due to the high concentration of H⁺. Consequently, fewer TiO₂ nanoclusters are formed, which is beneficial to crystal growth rather than aggregation and a product with large crystal size could be obtained. The added urea is decomposed and the produced NH₃•H₂O react with HCl as

shown in the equation (3) and (4). It is worth to point out that the acidity of reaction system is decreased, which would favor the formation of more TiO₂ nanoclusters and result in smaller crystalline sizes of product. [38, 39]



Fig. 2 depicts the SEM and TEM images of FNT-5. Fig. 3a is the low-magnification image of the as prepared FNT-5. It could be found that the as-prepared codoped sample consists entirely of small spherical particles with an average size of 200 nm to 2 μm. The Fig. 3b is the magnified surface morphologies of the typical codoped titania spheres showing the puckered surface of codoped titania. This unique morphology can endow the catalyst with more active sites and larger light-harvesting ability. This puckered surface of the codoped sphere is also shown in the TEM images. In Fig. 3d, well-resolved lattice fringes with an interplanar distance of 0.35 nm corresponding to the (101) d spacing of the anatase phase are clearly observed from the HRTEM images, further confirming the good crystallinity of as-prepared products.

Fig. 3 shows the SEM images of the products fabricated under different conditions. Interestingly, the presence of urea can affect the surface morphology of the product. In the case of the sample prepared without urea, it consists of spherical particles with a relative smooth surface morphology. While the solid spheres with puckered surface were obtained with the addition of urea, but the quantity of added urea seems to have no effect to the morphology of final products.

On the basis of the above discussion, we propose the possible mechanisms for the special morphology of codoped product prepared by the ultrasonic spray pyrolysis method. It is widely accepted that the droplets produced from nebulizer serve as microreactors and yield one particle per droplet when sprayed into a tubular reactor under pyrolysis condition. The size of droplet determines the product dimension. [40] The solvent was evaporated out of the droplets in the hot zone of the furnace, leading to the formation of microspheres. In this process, the hydrolysis velocity of Ti

source plays a vital effect to the structure. For the samples without urea, the hydrolysis of TiF_4 was restrained due to the low pH value of reaction system, so the hydrolysis of TiF_4 was happened after the volatilization of HCl in the aerosol (See scheme 1 (a)), hence forming a product with hollow structure (see Fig S1 (a)). While for the codoped samples, the formation process may follow the route shown in Scheme 1 (b). The urea react with HCl in the precursor solution. As the TiF_4 was unstable, it can be under hydrolysis easily before the volatilization of liquid in the aerosol, hence getting the solid sphere (see Fig S1 (b)). In addition, the surface of the products have distinct different morphologies under different preparation conditions For the fluorine and nitrogen codoped samples, the urea in the precursor was decomposed easily and formed NH_4Cl according to reaction of eq. (3) and (4). The NH_4Cl left in the sphere would be decomposed (eq. (5)) at high temperature and cause the shrink of the forming sphere with puckered surface. The NH_3 from the decomposed NH_4Cl and HF leads to the hydrolysis of TiF_4 , which would react with TiO_2 under high temperature (eq. (6)) and consequently from the codoped catalyst.



The UV/Vis spectra of the prepared samples were recorded through the diffuse reflectance technique with the pure TiO_2 (P25, Degussa) as comparison. The result is shown in the Fig. 4. Comparing with commercial TiO_2 (P25, Degussa), the doped TiO_2 spheres reveal a new absorption shoulder at 400-600 nm in the UV-vis spectrum. The single doping of fluorine only have limited influence to light absorption properties of titania, which only have a small shoulder at 400-450 nm. The F-doped- TiO_2 hollow spheres exhibit a slight tinge of light yellow color which could be due to the surface oxygen vacancies generated by the doping of fluorine. [41, 42] In comparison, the codoped samples have yellow color and show a remarkable shift to visible-light region. Two optical absorption thresholds at about 535 and 440 nm in the visible range were observed for all the codoped TiO_2 . These two absorption thresholds also demonstrate that two possible compositions have been

introduced to TiO₂. The absorption threshold at about 440 nm is ascribed to the introduction of nitrogen to the TiO₂ lattice. The absorption edge of this band shifts towards higher wavelength with increasing urea concentration in the precursor for all the codoped titania photocatalysts. The difference of the shift is due to the different amount of nitrogen doped into the TiO₂ framework as shown in XPS results. The absorption thresholds at about 535 nm are the superposition result of the nitrogen and fluorine doped into TiO₂ lattice. This enlarged light absorption range for the codoped samples in visible region have great influence to their photocatalytic property.

The assessment of the surface chemical composition and electronic state of the product were investigated by XPS analysis. The surface concentrations of fluorine and nitrogen in these photocatalysts are summarized in Table 1. It could be found that the fluorine and nitrogen concentrations increased with i urea concentration in the precursor. It was obvious that the increased N dopant is due to the nitrogen resource from urea. While for the fluorine, the HF in the codoped system may react with the NH₃ which was produced by the urea decomposition forming NH₄F. The boiling point of NH₄F (64.6 °C) is much higher than that of HF (19.4 °C). This could reduce the fluorine species losing by the evaporation in the reaction. Thus more fluorine will dope into TiO₂ with the increase amount of urea. The high-resolution XPS spectra of N1s and F1s are shown in Fig. 5 and Fig. 6, respectively. The N 1s regions of all samples are asymmetric, indicating that there are at least two kinds of chemical states. N 1s region could be fitted into two peaks. The binding energy region near 399.5 eV is derived from the presence of O–Ti–N linkages in the crystalline TiO₂ lattice. [43] It has been proved that this nitrogen state can be responsible for the observed shift of the photochemical threshold of TiO₂. [44, 45] While the N 1s peaks at 401.6 eV are arisen from the N atoms of adventitious N–N, N–O, or NHX adsorbed on the surface of the sample.[46-48] Fig. 6 gives the F 1s XPS spectra with wide and symmetrical peaks at 685 eV were observed, which could be assigned to the substitutional fluorine in titania lattice. [49]

The oxidation of NO under the irradiation of visible light was used to evaluate the photocatalytic activity of the samples prepared under different conditions. It is found that NO could be oxidized over the catalysts prepared under different conditions when the visible light was switched on. The control experiment found that the photolysis of NO without photocatalysts or use pure TiO₂ (P25) was negligible. Consequently, it could be concluded that all the samples have visible-light-driven photocatalytic activity. Table 2 shows the photocatalytic activity of codoped TiO₂ for NO oxidation under visible light. Compared with the fluorine single doped sample, the codoping greatly affects the photocatalytic activity of spherical TiO₂ toward oxidizing NO in gas-phase. For the single fluorine doping sample, the NO photocatalytic oxidation rate is 190.7 μ mol/mol·h. The oxygen vacancy created by the doped fluorine slightly extended the optical absorption of TiO₂ in the visible-light region, which contributes to the visible-light photocatalytic activity of fluorine doping sample. [50] However, the activity of single doping is limited as the doping of fluorine could not alter the basic band structure of TiO₂. For the codoped samples, they show high oxidation rate under optimal condition. For the sample of FNT-10, the NO photocatalytic oxidation rate is 287.4 μ mol/mol·h, which is about 50 % higher than that of FT. The enhanced activity of FNT-10 can be ascribed to the following two reasons. First the improved visible-light absorption and red shift of codoped TiO₂ which would lead to increased number of photons that taking part in the photocatalytic reaction. Second, the small crystal size of codoped TiO₂ is benefit to its photocatalytic performance. With a smaller particle size, the number of active surface sites increases and so does the surface charge carrier transfer rate in photocatalysis. Therefore the higher photocatalytic performance is obtained [51].

The results also show that the activities of codoped samples were greatly influenced by the amount of urea added in the precursor solution. The photocatalytic activity of samples decreased with the amount of urea added. This is due to more fluorine and nitrogen atoms were doped into

TiO₂ lattice as well as the smaller crystalline sizes for the samples prepared with more urea in the precursor. While if we further increased the amount of urea (>10 g) in the preparation, the precursor solution was not stable and some sedimentation was formed, thus we could not get the codoped TiO₂ with ultrasonic spray pyrolysis method.

4. Conclusion

In summary, the fluorine and nitrogen codoped TiO₂ spheres with puckered surface was fabricated via ultrasonic spray pyrolysis method. Increasing the concentration of urea added can increase the amount of nitrogen and fluorine doped into TiO₂ lattice, resulting in a new strong absorption band in the visible range. Activity test shows that the fluorine and nitrogen codoped TiO₂ could efficiently photocatalytic oxidize the NO under visible-light irradiation. The activity of codoped sample was higher than that of fluorine doped TiO₂. This facile method may be easily scaled up for industrial production. Similar doping or codoping with other nonmetal and metal ions (S, Cl, Br, B, Pt and Fe) with this method could lead to the development of new kind of spherical semiconductor composites, which are promising candidates as multifunctional materials as catalysts, photocatalysts and optoelectronic materials.

Acknowledgment

This work was supported by the Research Grants Council of Hong Kong (PolyU5204/07E) and the Hong Kong Polytechnic University (GYX0L, GYF08 and GYX75), National Natural Science Foundation of China (21103095) and the Natural Science Foundation of Fujian Province (Grant No. 2010J05030)

Reference:

- [1] J. Heinrich, *Int. J. Hyg. Envir. Heal.* 214 (2011) 3-27.
- [2] C. Nguyen, C. G. Sonwane, S. K. Bhatia, D. D. Do, *Langmuir* 14 (1998) 4950-4952.
- [3] E. N. Coker, C. Jia, H. G. Karge, *Langmuir* 16 (2000) 1205-1210.
- [4] K. Yu, G. W. M. Lee, *Appl. Catal. B: Environ.* 75 (2007) 29-38.
- [5] M. Koch, D. R. Cohn, R. M. Patrick, M. P. Schuetze, L. Bromberg, D. Reilly, K. Hadidi, P. Thomas, P. Falkos, *Environ. Sci. Technol.* 29 (1995), 2946-2952.
- [6] J. C. Yu, J. G. Yu, L. Z. Zhang, W. K. Ho, *J. Photochem. Photobio. A Chem* 148 (2002) 263-271.
- [7] H. F. Xu, G. Vanamu, H. Konishi, R. Yeredla, J. Phillips, Y. F. Wang, *J. nanometer.* 2 (2006) article ID.
- [8] J. G. Yu, H. G. Yu, B. Cheng, X. J. Zhao, Q. J. Zhang, *J. Photochem. Photobio. A Chem* 182 (2006) 121-127.
- [9] X. F. Chen, X. C. Wang, X. Z. Fu, *Energ. Environ. Sci* 2 (2009) 872-877.
- [10] K. Wilke, H. D. Breuer, *J. Photochem. Photobio. A Chem* 121 (1999) 49-53.
- [11] J. S. Zhang, X. F. Chen, K. Takanabe, K. Maeda, K. Domen, J. D. Epping, X. Z. Fu, M. Antonietti, X. C. Wang, *Angew. Chew. Int. Edit.* 49 (2009) 441-444
- [12] H. Irie, S. Washizuka, N. Yoshino, K. Hashimoto, *Chem. Commun.* (2003) 1298-1299.
- [13] S. Horikoshi, Y. Minatodani, H. Sakai, M. Abe, N. Serpone, *J. Photochem. Photobio. A Chem.* 217 (2011) 191-200.
- [14] W. Guo, L. Q. Wu, Z. Chen, G. Boschloo, A. Hagfeldt, T. L. Ma, *J. Photochem. Photobio. A Chem.* 219 (2011) 180-187.
- [15] J. G. Yu, J. C. Yu, B. Cheng, S. K. Hark, K. Iu, *J. Solid State Chem.* 174 (2003) 372-380.
- [16] J. S. Jang, H. G. Kim, S. M. Ji, S. W. Bae, J. H. Jung, B. H. Shon, J. S. Lee, *J. Solid State Chem.* 179 (2006) 1067-1075.

- [17] Y. Xie, X. Zhao, Y. Chen, Q. Zhao, Q. Yuan, J. Solid State Chem. 180 (2007) 3576-3582.
- [18] J. C. Yu, W. K. Ho, J. G. Yu, H. Y. Yip, P. K. Wong, J. C. Zhao, Environ. Sci. Technol. 39 (2005) 1175-1179.
- [19] R. Asahi, T. Morikawa, T. Ohwaki, K. Aoki, Y. Taga, Science 293 (2001) 269-271.
- [20] H. Irie, Y. Watanabe, K. Hashimoto, J. Phys. Chem. B 107 (2003) 5483-5486.
- [21] Q. C. Xu, D. V. Wellia, S. Yan, D. W. Liao, T. M. Lim, T. T. Y. Tan, J. Hazard. Mater. 188 (2011) 172-180.
- [22] J. A. Rengifo-Herrera, K. Pierzchala, A. Sienkiewicz, L. Forro, J. Kiwi, J. E. Moser, C. Pulgarin, J. Phys. Chem. C 114 (2010) 2717-2723.
- [23] H. J. Tian, L. H. Hu, W. X. Li, J. Sheng, S. Y. Xu, S. Y. Dai, J. Mater. Chem. 21 (2011) 7074-7077.
- [24] R. Long, N. J. English, J. Phys. Chem. C 114 (2010) 11984-11990.
- [25] W. Ho, J. C. Yu, S. C. Lee, Chem. Commun. (2006) 1115-1117.
- [26] Y. L. Su, X. W. Zhang, M. H. Zhou, S. Han, L. C. Lei, J. Photochem. Photobio. A Chem 194 (2008) 152-160.
- [27] D. Li, H. Haneda, S. Hishita, N. Ohashi, J. Solid State Chem. 178 (2005) 3293-3302.
- [28] S. Livraghi, K. Elghniji, A. M. Czoska, M. C. Paganini, E. Giamello, M. Ksibi, J. Photochem. Photobio. A Chem 205 (2009) 93-97.
- [29] D. G. Huang, S. J. Liao, J. M. Liu, Z. Dang, L. Petrik, J. Photochem. Photobio. A Chem. 184 (2006) 282-288.
- [30] J. Xu, B. F. Yang, M. Wu, Z. P. Fu, Y. Lv, Y. X. Zhao, J. Phys. Chem. C 114 (2010) 15251-15259
- [31] G. W. Koebrugge, L. Winnubst, A. J. Burggraaf, J. Mater. Chem. 3 (1993) 1095-1112.
- [32] S. J. Kim, S. D. Park, Y. H. Jeong, S. Park, J. Am. Ceram. Soc. 82 (1999) 927-932.

- [33] H. B. Yin, Y. Wada, T. Kitamura, S. Kambe, S. Murasawa, H. Mori, T. Sakata, S. Yanagida J. Mater. Chem. 11 (2001) 1694-1703.
- [34] S. E. Skrabalak, K. S. Suslick, J. Phys. Chem. C 111 (2007) 17807-17811.
- [35] K. D. Kim, K. Y. Choi, J. W. Yang, Colloids Surf. A 254 (2005) 193-198.
- [36] Z. Ai, L. Zhang, S. Lee, J. Phys. Chem. C 114 (2010) 18594-18600.
- [37] Y. Huang, Z. Ai, W. Ho, M. Chen, S. Lee, J. Phys. Chem. C 114 (2010) 6342-6349.
- [38] X. Z. Li, F. B. Li, Environ. Sci. Technol. 35 (2001) 2381-2387.
- [39] M. Zhou, J. Yu, H. Yu, J. Mol. Catal. A: Chem. 313 (2009) 107-113.
- [40] J. Zhang, A. Elsanousi, J. Lin, Y. Huang, E. M. Elssfah, D. Chen, J. Gao, Z. Huang, X. Ding, C. Tang, Cryst. Growth Des. 7 (2007) 2764-2767.
- [41] A. G. Kontos, M. Pelaez, V. Likodimos, N. Vaenas, D. D. Dionysiou, P. Falaras, Photochem. Photobiol. Sci. 10, (2011) 350-354
- [42] I. N. Martyanov, S. Uma, S. Rodrigues, K. J. Klabunde, Chem. Commun. (2004) 2476-2477
- [43] T. L. Ma, M. Akiyama, E. Abe, I. Imai, Nano. Lett. 5 (2005) 2543-2547.
- [44] O. Diwald, T. L. Thompson, T. Zubkov, E. G. Goralski, S. D. Walck, J. T. Yates, Jr., J. Phys. Chem. B 108 (2004) 6004-6008.
- [45] J. Fang, F. Shi, J. Bu, J. Ding, S. Xu, J. Bao, Y. Ma, Z. Jiang, W. Zhang, C. Gao, W. Huang, J. Phys. Chem. C 114 (2010) 7940-7948.
- [46] J. L. Gole, J. D. Stout, C. Burda, Y. Lou, X. Chen, J. Phys. Chem. B 108 (2004) 1230-1240.
- [47] S. Sakthivel, H. Kisch, ChemPhysChem 4 (2003) 487-490.
- [48] J. A. Rodriguez, T. Jirsak, J. Hrbek, J. Dvorak, A. Maiti, J. Am. Chem. Soc. 123 (2001) 9597-9605.
- [49] D. Li, H. Haneda, S. Hishita, N. Ohashi, Mater. Sci. Eng. B 117 (2005) 67-75.
- [50] D. Li, H. Haneda, S. Hishita, N. Ohashi, Chem. Mater. 17 (2005) 2596-2602.

[51] J. Zhu, J. Yang, Z. F. Bian, J. Ren, Y. M. Liu, Y. Cao, H. X. Li, H. Y. He, K. N. Fan Appl. Catal.

B: Environ. 76 (2007) 82–91

Figure caption:

Fig. 1. The X ray diffraction patterns of fluorine-doped and fluorine and nitrogen codoped TiO₂ prepared at different conditions.

Fig. 2. The morphology and structural characterization of FNT-5: (a) SEM image; (b) Magnified SEM image; (c) TEM image; (d) HRTEM image.

Fig. 3. SEM images of fluorine and nitrogen codoped TiO₂ with different amount urea in the precursor solution: (a) FT ; (b) FNT-1 ; (c) FNT-5; (d) FNT-10. The scale bar in the figure is 1 μm.

Fig. 4. UV-vis diffuse reflectance spectra of fluorine and nitrogen codoped TiO₂ with different urea in the precursor solution with pure TiO₂(P25) as comparasion.

Fig. 5. The F1s spectra of fluorine and nitrogen codoped TiO₂ with different urea in the precursor solution.

Fig. 6. The Ti2p spectra of fluorine and nitrogen codoped TiO₂ with different urea in the precursor solution.

Table 1 The quantitative XPS analysis result using the appropriate molar weight-correction factors.

Table 2 The photocatalytic oxidation rate of NO under the irradiation of visible light over the catalyst prepared under different conditions.

Scheme 1 Schematically illustrating the structure formation of FT and FNT via the ultrasonic spray pyrolysis process.

Fig. 1.

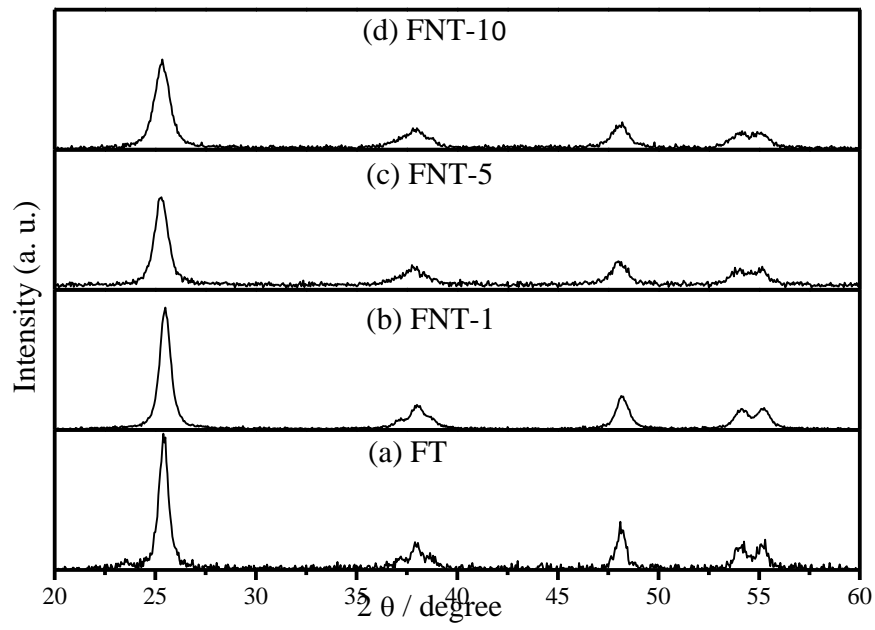


Fig. 2.

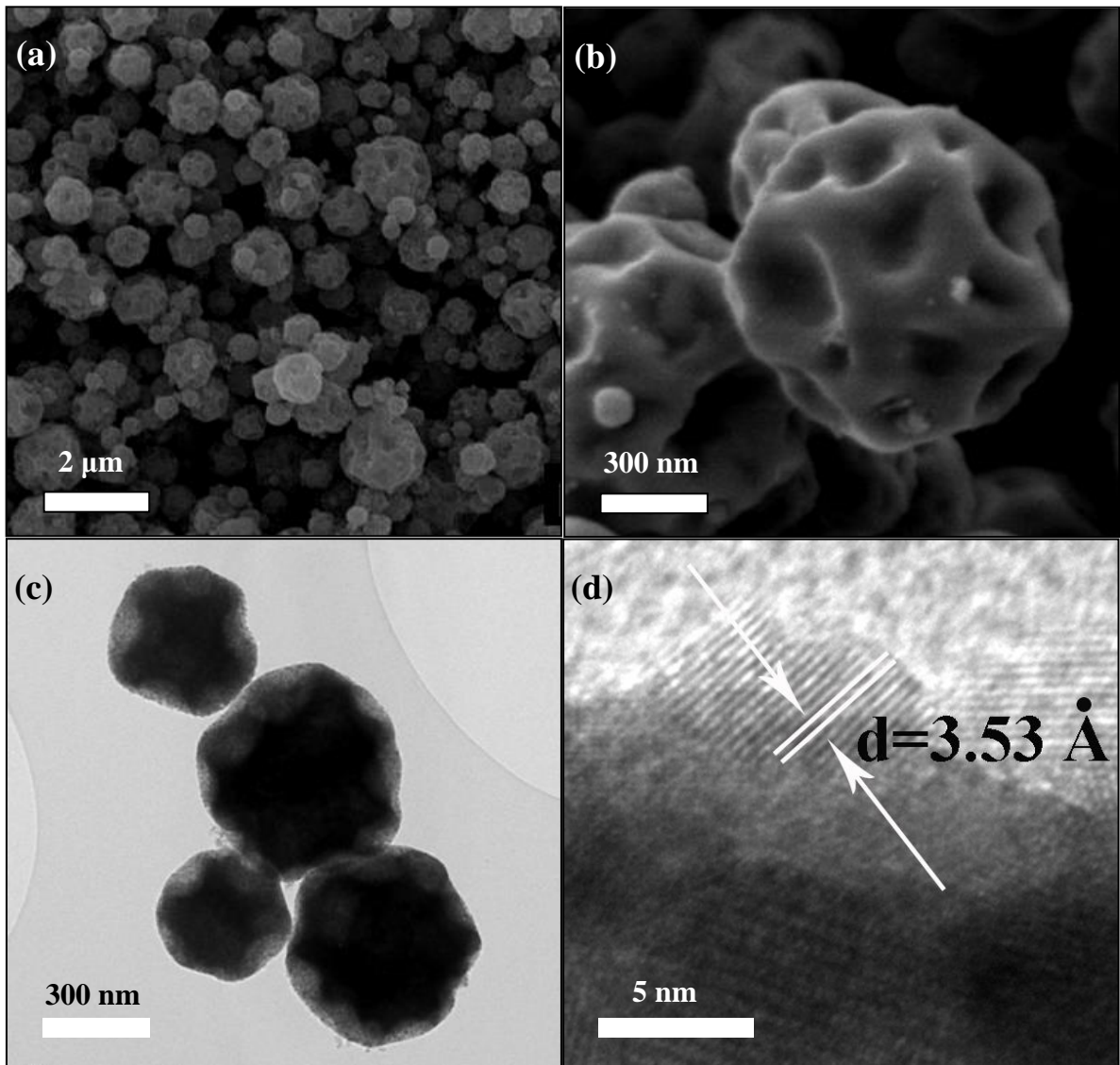


Fig. 3.

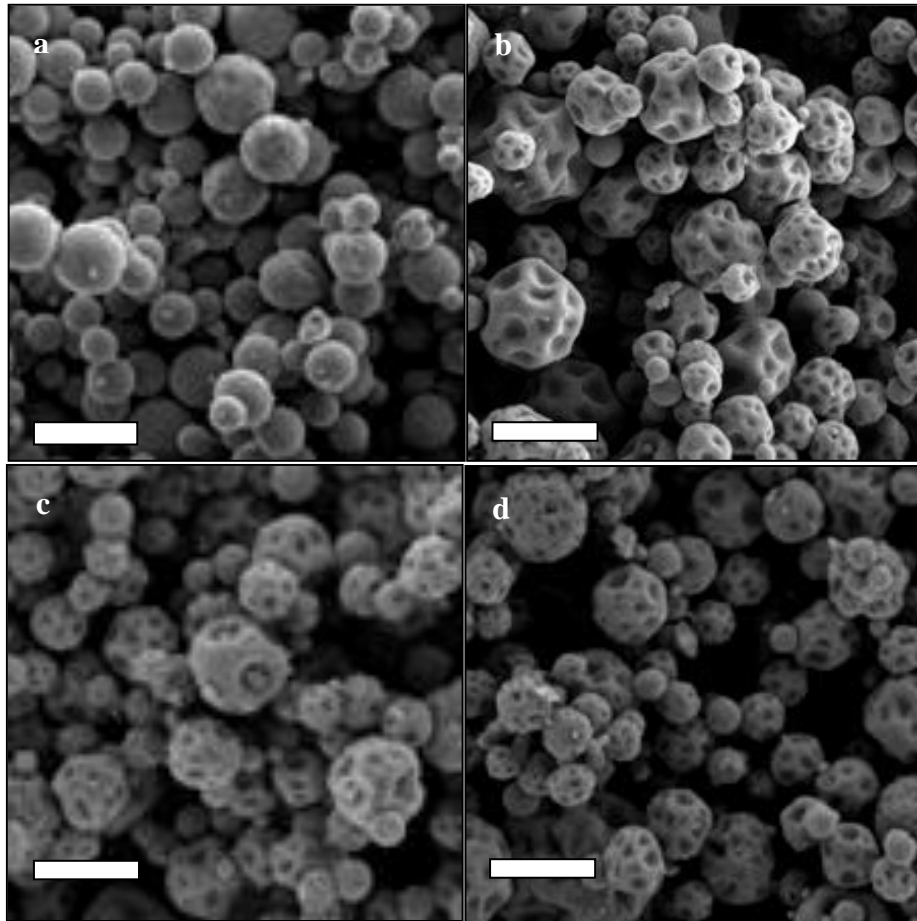


Fig. 4.

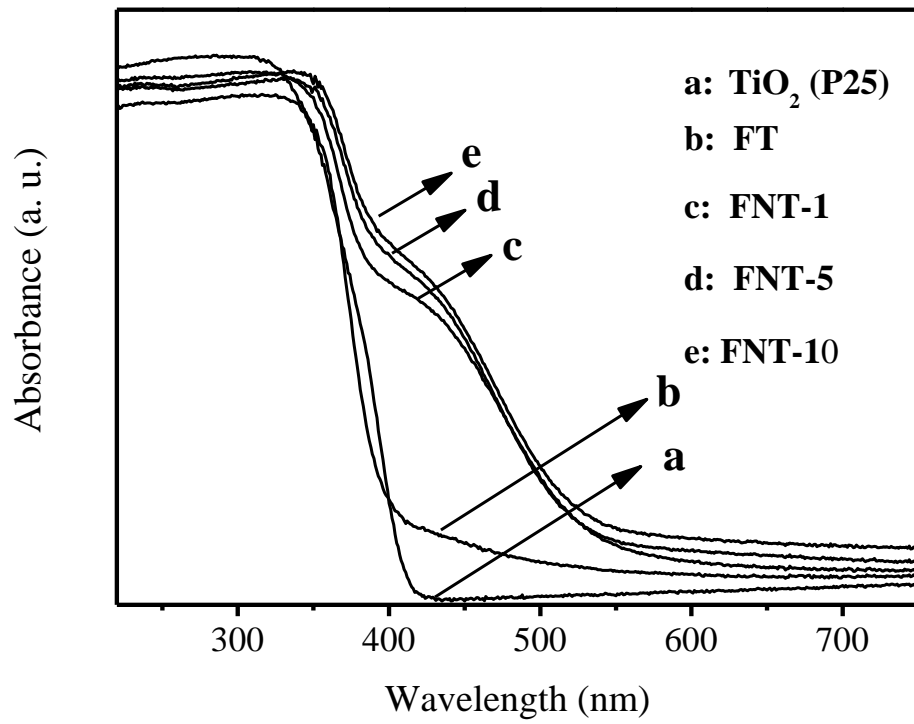


Fig. 5.

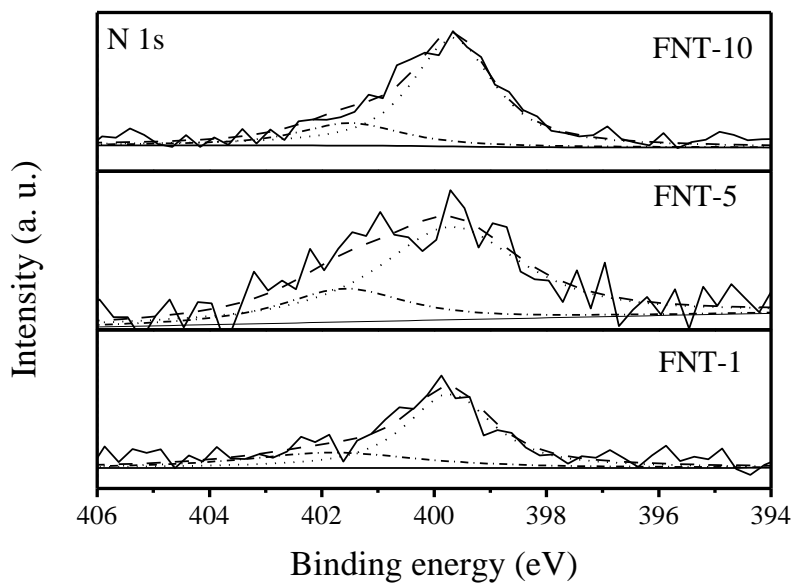


Fig. 6.

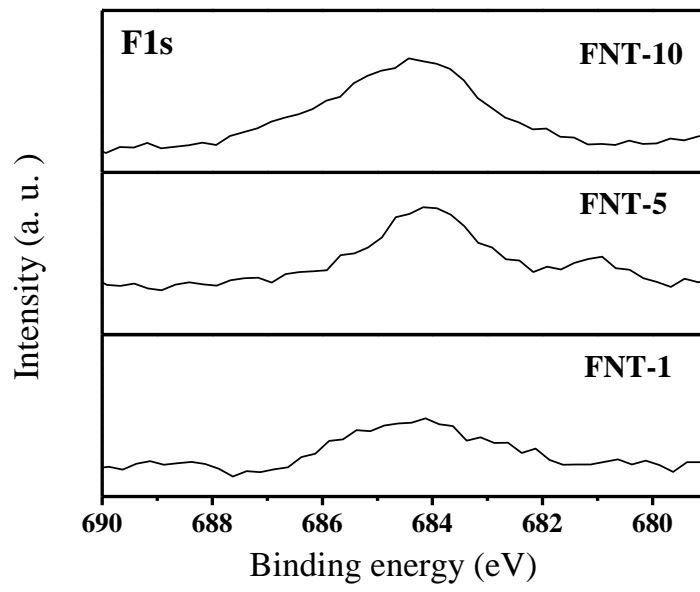


Table 1

Sample name	F atomic conc.	N atomic conc.
FT	4.0%	-
FNT-1	1.46%	1.38%
FNT-5	1.62%	2.38%
FNT-10	1.81%	3.65%

Table 2

Sample name	FT	FNT-1	FNT-5	FNT-10
Oxidation rate ^a	190.7	142.1	198.1	287.4

^a Oxidation rate: n(nitric oxide) per mol of catalyst per hour (μ mol/mol·h).

Scheme 1

